ORIGINAL RESEARCH ARTICLE

Organic and Hybrid Diode Features of an *n*-Type 1,8-Naphthalimide Derivative

Sneha Kagatikar[1] · Parashurama Salunkhe[2] · Dhanya Sunil[1] · Dhananjaya Kekuda[2]

Abstract

Organic–inorganic hybrid photodiodes have garnered research interest to achieve high-performance optoelectronic devices with longer lifetime. In the present study, a fluorescent 1,8-naphthalimide (NI) derivative BHSHNI was synthesized through bromination of 3-hydroxy naphthalic anhydride and subsequent imidation reaction with salicyloyl hydrazide. The IR, NMR and mass spectrometry studies confirmed the molecular structure of the NI derivative. Intramolecular charge transfer was confirmed using theoretical and fluorescence emission studies. Thermal investigations suggested good stability of BHSHNI and cyclic voltammetry indicated an electrochemical band gap of 1.10 eV. Surface uniformity and pit-free morphology was observed in SEM and AFM images of thin films formed by BHSHNI. The organic (PEDOT:PSS) and hybrid (organic–inorganic) *p–n* type diodes were successfully constructed using BHSHNI. The hybrid diode exhibited better features with ideality factors of 9.3 and 15.2 in dark and visible light, respectively, with a dielectric constant of 7.65 at 30 kHz. The calculated responsivity of the hybrid diode was found to be 66.26 μA/W. The device incorporating BHSHNI as functional material with NiO can be further explored for photodiode applications.

Graphical Abstract
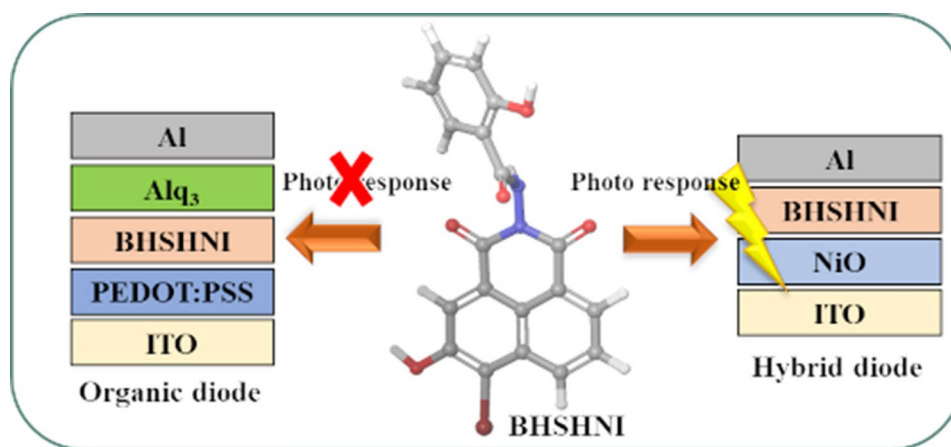
Keywords 1,8-Naphthalimide · organic and hybrid diodes · electron transport layer

✉ Dhanya Sunil
dhanyadss3@gmail.com

1 Department of Chemistry, Manipal Institute of Technology, Manipal Academy of Higher Education, Manipal, Karnataka 576104, India

2 Department of Physics, Manipal Institute of Technology, Manipal Academy of Higher Education, Manipal, Karnataka 576104, India

Introduction

Research on inorganic materials for electronic devices has progressed dramatically in recent years due to their versatile properties and high efficiency. However, organic electronics such as transistors,[1–4] photovoltaics,[5,6] and thermoelectric

devices[7] have attracted wide attention among researchers to achieve the desired device properties at a considerably reduced cost. Thus, organic electronics have evolved as an active, advanced, easy and high-performance modern technology. Among the electronic devices, the semiconductor diode is a two-terminal electrical device with a *p–n* junction, mainly used as inverters and rectifiers in power supply structures, clamping devices and logic gates in computer systems, limiters, clippers and gates in optical communication systems, and phase clamping devices, limiters, and detectors in televisions. They are also used in biomedical imaging, environmental monitoring, and sensing.[8,9] A photodiode (PD) generates electrical signals when illuminated with light and is mainly used as a photodetector. The charge transport properties of the sandwich structures, which form an integral part in diodes are very crucial in PDs. There is much scope to improve the electrical transport features of the functional materials by using suitable injection and transport materials in these devices. Moreover, it is imperative to analyze the effect of charge transport properties of organic and inorganic materials in sandwich structures.

Organic molecules are primarily used in PDs because of their low-cost manufacturing, inherent tunability to detection wavelength, and compatibility with flexible devices.[10] Although certain inorganic metals seem promising, their intrinsic drawbacks including broadband absorption, high brittleness, complicated and expensive manufacturing process, and potential toxicity limit their applicability.[11,12] Lower charge carrier mobility and less-ordered molecular arrangement of organic molecules result in slower response speed and fewer charge generation in PDs compared to their inorganic counterparts. Hence, in some devices, blends of organic and inorganic materials are also used.

In recent years, researchers are immensely interested in the electrochemical, optical, as well as photoelectric aspects of electron-deficient 1,8-naphthalimides (NI), which possess a rigid planar framework.[13] These derivatives possess a structure with an electron-deficient center and good thermal stability, which are the two primary requirements for an electron transport material. Most NI derivatives display high solid state fluorescence quantum yield and have been employed as electron-deficient materials in organic light emitting diodes with good performance and electroluminescence stability.[14] NI derivatives serve as excellent electron conductors and are used as host or electron transport materials.[15,16] As these materials can exhibit low reduction potentials[15,17,18] and wide energy gaps,[19–21] they are studied for their application as electron-deficient *n*-type organic semiconductors.[22–24] Therefore, in the present study a NI derivative, BHSHNI has been synthesized through easy synthetic protocols as an *n*-type semiconductor material in the fabrication of two types of diodes: organic with PEDOT:PSS and hybrid with nickel(II) oxide as *p*-type materials.

Materials and Methods

Chemicals/solvents procured from Sigma Aldrich, TCI Chemicals, and Finar were used in the experiments. The open capillary method was used to determine the melting point and is uncorrected. The infrared (IR) and nuclear magnetic resonance (NMR) (^{1}H and ^{13}C) spectra were obtained using Shimadzu FTIR and Bruker 400 MHz spectrophotometers. The mass spectrum was acquired with electrospray ionization by means of an Agilent 6430 Triple Quad instrument. An 1800 Shimadzu UV–visible spectrophotometer was used to record the absorbance spectra. The thermal study was performed using a Hitachi STA7000 series thermal analyzer under nitrogen atmosphere at a heating rate of 10°C min^{-1}. The B3LYP functions of Schrödinger's Materials Science Suite (6-31G^{++} basis set) were employed for the computational studies. Cyclic voltammetry (CV) measurements were performed at 50 mV s^{-1} scan rate using a CH Instrument 604E series (USA) with Beta software. The conventional cell system comprising glassy carbon (0.0771 cm^2 electroactive area) as the working electrode, platinum wire as the auxiliary electrode and Ag/AgCl(KCl$_{sat}$) as the reference electrode were dipped in tetrabutylammonium hexafluorophosphate in acetonitrile (0.1 M) as the supporting electrolyte. Hall effect experiment and dielectric studies were performed using a Keithley Hall Effect setup 3706A and a Hioki LCR meter IM 3635, respectively. A Carl Zeiss EVO 18 analytical scanning microscope (SEM) and an INNOVA SPM atomic force microscope (AFM) were used to analyze the surface morphology of the thin films.

A *p–n* type organic diode was fabricated using BHSHNI as *n*-type material and PEDOT:PSS as *p*-type material. Further, a hybrid diode was prepared by replacing PEDOT:PSS with NiO as the *p*-type material. NiO thin film was deposited on ITO glass substrate using reactive DC magnetron sputtering, and the film was grown using a 99.99% pure nickel metallic target of 2-inch diameter. The vacuum chamber was sustained at $\sim 7 \times 10^{-4}$ Pa, and a mixed ambience of Ar/O$_2$ ratio of 6/1 sccm (standard cubic centimeters per minute) was maintained during the deposition. The sputter power to the nickel target was fixed at 50 W and sputtering was performed at 1 Pa. The crystallinity of the NiO film was examined by x-ray diffraction (XRD, Rigaku MiniFlex) using monochromatic Cu-Kα radiation, and thickness was measured using a stylus profilometer (DektakXT, Bruker). The I–V measurements of the diode were performed using a Keithley 2400 source meter.

Scheme. 1. Synthetic route of
NI derivative.

BHNI

BHSHNI Br
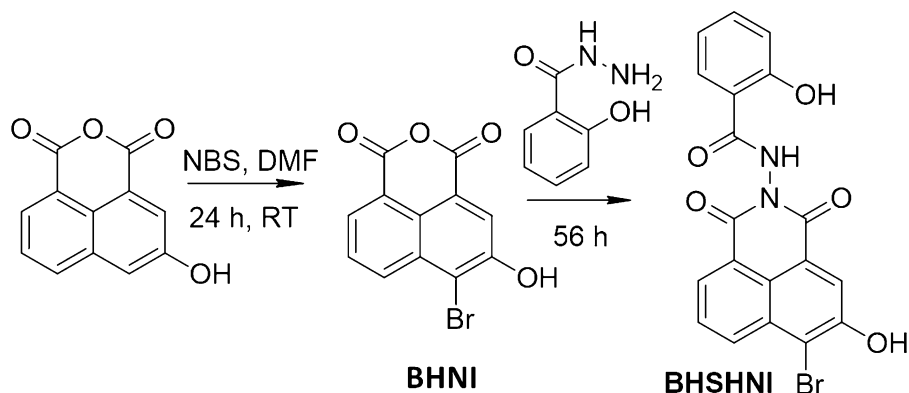
Results and Discussion

Synthesis and Characterization of BHSHNI

The synthesis of the NI derivative involves two-steps: the initial bromination reaction of 3-hydroxy-1,8-naphthalic anhydride and subsequent imidation with salicyloyl hydrazide. The synthetic pathway for BHSHNI is depicted in Scheme 1.

6-bromo-5-hydroxybenzo[de]
isochromene-1,3-dione(BHNI)

N-Bromosuccinimide (NBS: 2 mmol) in DMF was added to 3-hydroxy-1,8-naphthalic anhydride (2 mmol) in DMF and refluxed at room temperature (RT) for 24 h. The reaction mixture was quenched in ice, filtered, and dried to obtain BHNI.

N-(6-bromo-5-hydroxy-1,3-dioxo-1H-benzo[de]isoqui-
nolin-2(3H)-yl)-2-hydroxybenzamide (BHSHNI)

Salicyloyl hydrazide (5 mmol) was added to BHNI (5 mmol) in ethanol and refluxed for 56 h, then cooled to RT to yield crude BHSHNI, which was further recrystallized in ethanol.

The molecular structure of the NI derivative was further confirmed using spectral techniques.

N-(6-bromo-5-hydroxy-1,3-dioxo-1H-benzo[de]
isoquinolin-2(3H)-yl)-2-hydroxybenzamide (BHSHNI):
Deep yellow powder (69%) mp: > 250℃; FT-IR (ATR, cm^{-1}) (Fig. S1): 3300 (OH *str.*), 3201 (NH *str.*), 3038 (Ar CH *str.*), 1716, 1691 (C=O *str.*); ^{1}H NMR (DMSO-d$_6$, 400 MHz) (Fig. S2): δ 6.998–7.065 (m, 2H), 7.495–7.538 (m, 1H), 7.953–7.992 (m, 2H), 8.276 (s, 1H), 8.432–8.452 (dd, 1H,), 8.540–8.563 (dd, 1H); ^{13}C NMR (DMSO-d$_6$, 100 MHz) (Fig. S3): δ 113.64, 115.60, 117.78, 119.85, 122.23, 122.51, 122.58, 123.06, 129.40, 129.54, 130.07, 132.55, 132.64, 134.97, 154.24, 158.87, 161.54, 161.82, 166.55; MS C$_{19}$H$_{11}$O$_5$N$_2$Br (m/z) (Fig. S4): 427.

Photophysical Studies

Since light absorption in naphthalimides with *D–π–A* architecture generates charge transfer interactions between the carbonyl groups and the substituents at the *C*-4 position, their photophysical characteristics are mainly connected to the polarization of the chromophoric system.[25,26] The absorption spectrum of BHSHNI in DMSO (1×10^{-4} M) presented in Fig. S5A suggested two absorptions at 342 and 391 nm for *π–π** and *n–π** transitions.[27,28] The Tauc plot (Fig. S5B) with energy versus α h$\nu^{1/2}$ was used to estimate the optical band gap of BHSHNI, which was found to be 2.87 eV. The molar extinction coefficient (*ε*), which defines the amount of light absorbed by BHSHNI was calculated using Eq. 1.

$$\varepsilon = A/mC \qquad (1)$$

where *A* is the absorbance, *m* is the path-length of the light and *C* is the concentration of BHSHNI.

The high log *ε* value of 6.540 suggests long-wavelength absorption bands due to a charge transfer through *π–π* transition. The optimized molecular geometry and HOMO and LUMO energy levels of BHSHNI were generated using Schrodinger material suite software to realize the electron density distributions. The charge distribution of HOMO was found to be localized on the hydroxybenzamide unit of the molecule, whereas the electronic cloud was distributed on the NI moiety in the LUMO, indicating an ICT process as shown in Fig. 1a. Generally, molecules that exhibit an ICT process show hypsochromic shifts with increase in the emission intensity upon adding a small amount of nonpolar solvent to its solution in a polar solvent. The THF solution of BHSHNI (1×10^{-4} M) exhibited a hypsochromic shift of ~10 nm with an increase in emission intensity upon increasing hexane fractions (0–90%) as portrayed

in Fig. 1b. The electron-deficient NI moiety acted as the acceptor, and the hydroxybenzamide unit served as the electron donor in the molecule.

Electrochemical Measurements

The charge injection capabilities and molecular orbital energy levels for the NI derivative have been investigated using CV measurements. The current versus voltage plot
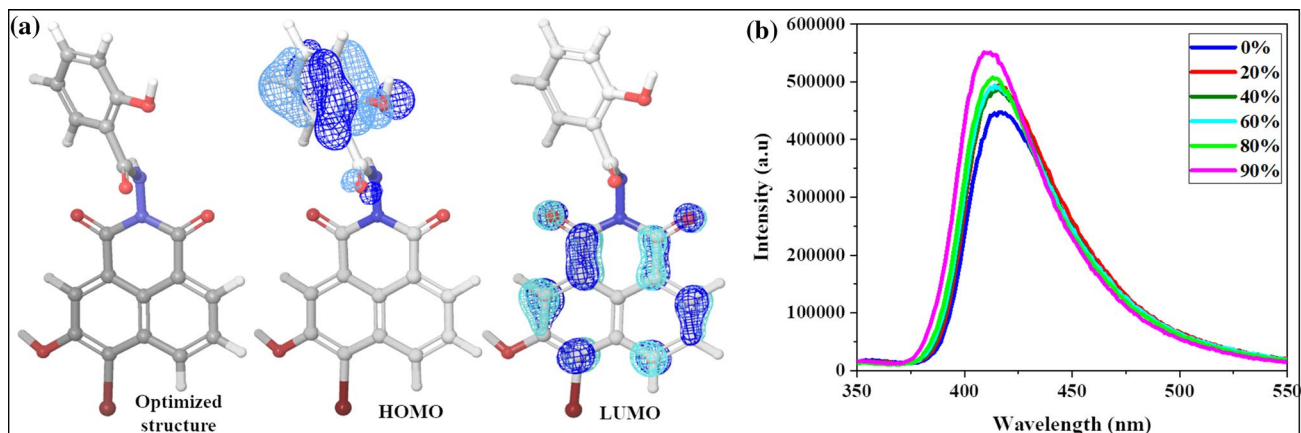

Fig. 1 (a) Theoretically obtained optimized geometry and molecular orbital structures of BHSHNI and (b) emission spectra of different hexane/THF solutions of BHSHNI.
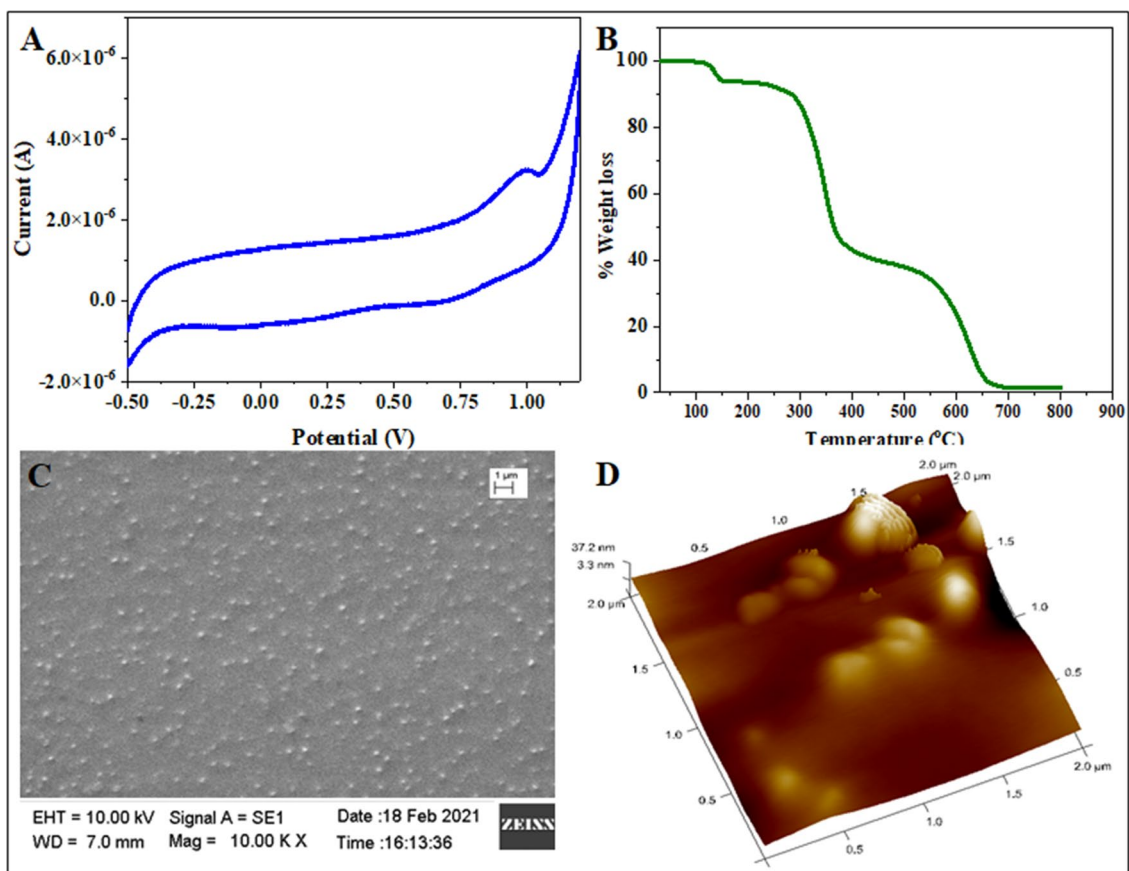
Fig. 2 (a) Cyclic voltammogram and (b) thermogram of BHSHNI. (c and d) SEM and AFM images of thermal evaporated thin films of BHSHNI.

demonstrated a redox peak between −0.5 eV and 1 eV at a scan rate of 20 mVs^{-1}. The cyclic voltammogram shown in Fig. 2a presented the oxidation and reduction onset potentials. The HOMO and LUMO levels of BHSHNI was calculated to be −5.303 eV and −4.2 eV, respectively, with a band gap of 1.10 eV. The LUMO level was quite low, indicative of an air-stable electron transport, suggesting that BHSHNI is a suitable candidate for device applications.

Thermal Analysis

Organic materials should possess significant thermal stability to endure temperature fluctuations to be employed in optoelectronic devices.[29–31] The TGA thermogram of BHSHNI was recorded from a temperature range of 50–800℃, and it was observed that the compound is thermally stable and degrades in three steps as depicted in Fig. 2b. The first step of degradation of 6% might be due to the lattice water molecules, and further weight losses of 47.6% and 37% could be attributed to molecular degradation.

Surface Analysis

The formation of uniform amorphous thin films is vital for any device application.[32] The surface morphology of the thermally evaporated thin film of BHSHNI was observed using SEM and AFM analysis. The SEM image, as depicted in Fig. 2c, showed the formation of a uniform thin film with pit-free surface. The AFM analysis (Fig. 2d) displayed a surface roughness (*Rq*) value of 3.79 nm, thereby supporting the SEM analysis data. These results indicate that BHSHNI is a suitable functional material for device fabrication with possibly reduced leakage of current.

Electrical Characterization

Various quantitative electrical parameters including charge mobility, charge carrier concentration and resistivity play an important role in interpreting the fundamental charge transport mechanisms and inherent mobility in organic semiconductors. NI derivatives are extensively researched as electron-deficient *n*-type organic semiconductors because they can have low reduction potentials and wide energy gap.[33–44] BHSHNI was found to be an *n*-type semiconductor with a charge carrier concentration of 1.57×10^{14} cm^{-3} and charge mobility of 7.06 cm^2/V s, which are favorable for different device applications.

Dielectric studies were accomplished in the frequency range of 10–5000 Hz by sandwiching the thermal evaporated BHSHNI (under vacuum 6×10^{-6} mbar) between the ITO coated plate and the aluminum contacts, which served as a parallel plate capacitor. The frequency-dependent capacitance measured (Fig. 3a) indicated a higher capacitance value at lower frequency, which dropped suddenly to attain a constant value. The higher values of capacitance could be attributed to major and minor carriers and interface states which respond to the AC. However, with increased frequency, only part of these interface states and major carriers respond to the AC current.[45] The interface states had enough time to capture the charges at lower frequencies, while charge trapping processes were sluggish at higher frequencies.[46]

The dielectric constant, which represents the ratio of permittivity of the dielectric material to that in free space, was calculated using Eq. 2 and plotted against frequency as shown in Fig. 3b.

$$\varepsilon_r = \frac{Cd}{\varepsilon_o A} \qquad (2)$$

where *C* is the capacitance, *d* represents thickness, ε_0 is the permittivity in free space and *A* signifies the active area.
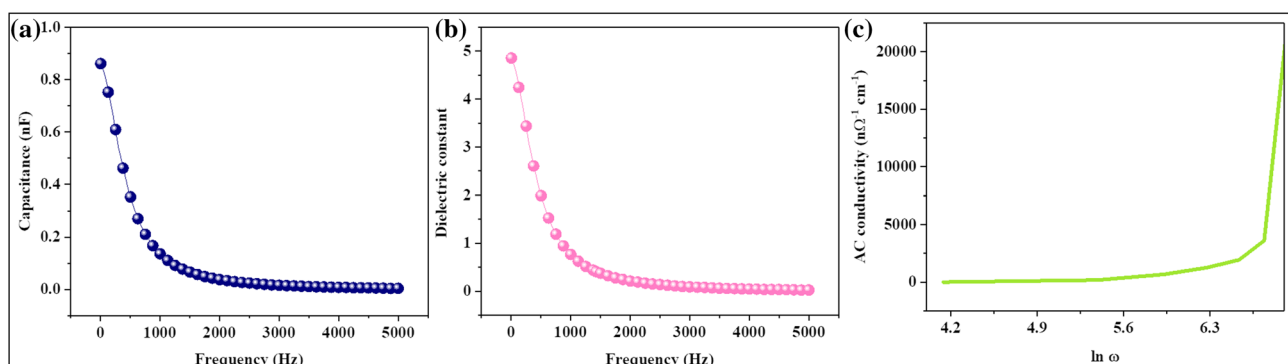

Fig. 3 (a) Capacitance versus frequency, (b) dielectric constant versus frequency, and (c) AC conductivity versus logarithm of angular frequency for BHSHNI.

The dielectric constant for BHSHNI was found to be 2.01 at 500 Hz. Electronic polarization and space charge could be responsible for the higher dielectric constants at lower frequencies.[47] The decline in the dielectric constant may be due to decrease in the polarization at higher frequencies.[48,49]

In an ideal case, charge should not penetrate through the dielectric material. However, large current flows through it upon applying potential, which is designated as dielectric loss. The dielectric loss versus frequency plot (Fig. S6) suggested minimal dielectric loss and storage of charges in the dielectric material, BHSHNI. As AC conductivity and dielectric loss are closely related, the increase in conductivity will increase the eddy current, which in turn will increase the dielectric loss.[45] AC conductivity was calculated using Eq. 3 and was plotted against semi logarithm of angular momentum as depicted in Fig. 3c. The AC conductivity of BHSHNI was found to be $\sim 15{,}000$ $n\Omega^{-1}$ cm^{-1} at higher frequencies.

$$\sigma_{AC} = \omega\varepsilon_o\varepsilon_r\tan\delta \tag{3}$$

where ω is the angular frequency, ε_o is the permittivity in free space, ε_r is the dielectric constant and $\tan\delta$ represents the dielectric loss of BHSHNI.

Diode Fabrication and Characterization

Organic Diode

A *p–n* type diode with ITO | PEDOT:PSS | BHSHNI | Alq3 | Al configuration was fabricated using BHSHNI as the active *n*-type component (Fig. 4a). The corresponding energy level diagram is displayed in Fig. 4b. PEDOT:PSS was spin-coated as a hole transport layer on precoated ITO plates, which acted as an anode, BHSHNI (100 nm) as *n*-type semiconductor, and Alq3 (60 nm) as the electron transport layer was thermal evaporated under a vacuum of 6×10^{-6} mbar with an evaporation rate of 0.1–0.5 Å/s. Al (100 nm) as cathode was coated on Alq3 by thermal evaporation at 1–5 Å/s to complete the device fabrication. The current versus voltage (I–V) plots were recorded for the device (Fig. 5a), and the current was observed in micro-amperes. The ideality factors calculated for the diode using log I versus voltage plot (Fig. 5b) for dark and visible light were found to be 27.6 and 14. The constructed diode did not exhibit a significant difference in the current value in dark and light conditions as evident from Fig. 5a and b.
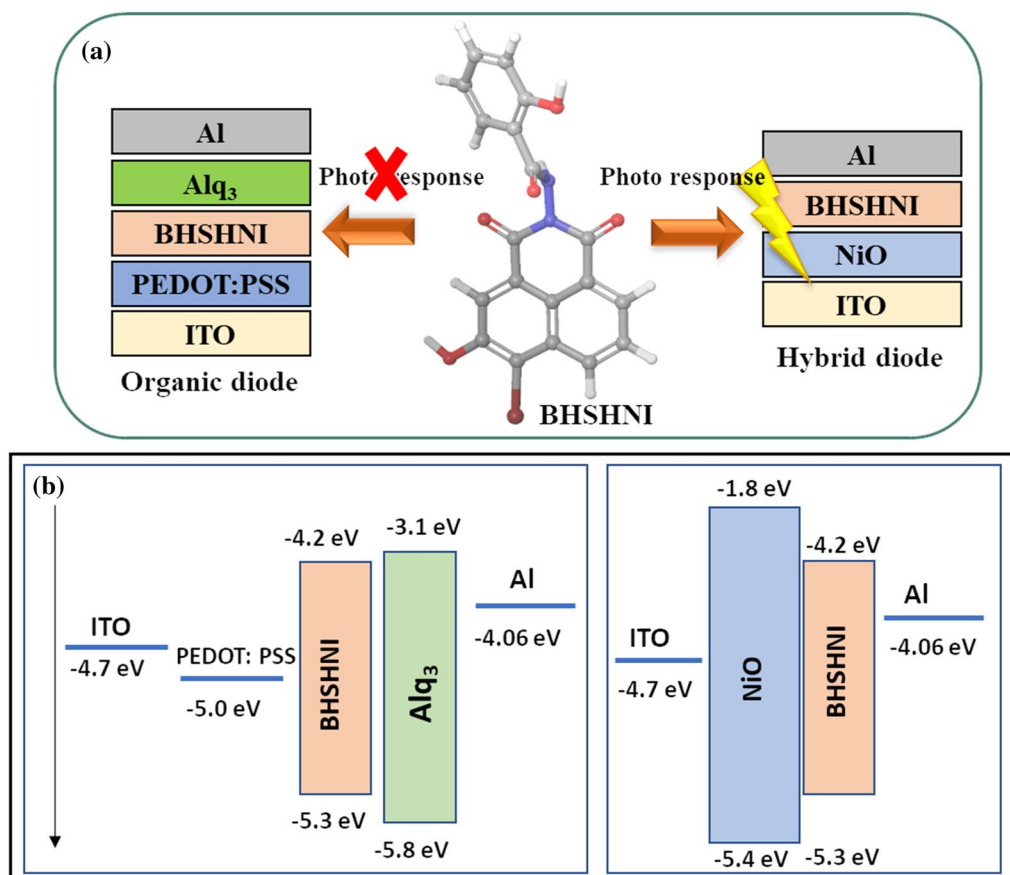

Fig. 4 (a) Device architectures and (b) energy level diagrams of different layers used in organic and hybrid diodes.
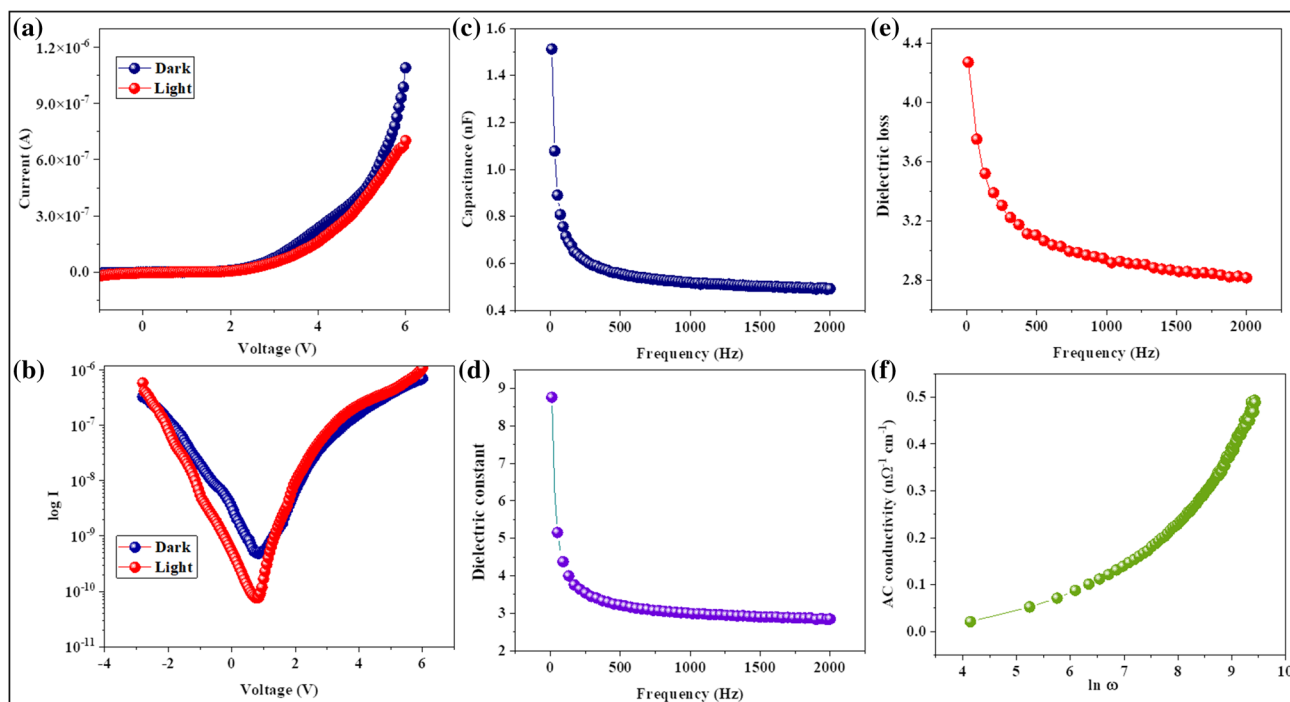
Fig. 5 The plots of (a) I–V, (b) log I versus V in light and dark conditions, (c) capacitance against frequency, (d) dielectric constant against frequency, (e) dielectric loss against frequency and (f) AC conductivity against logarithm of angular frequency for the diode with BHSHNI as the active material.

Further, the dielectric studies of the device with BHSHNI were performed from 10–1000 Hz where ITO plate and Al acted as parallel plates in a capacitor. Frequency-dependent capacitance plots were constructed as depicted in Fig. 5c, which displayed a capacitance of ~ 0.5 nF at higher frequencies. Furthermore, the dielectric constant versus frequency plot (Fig. 5d) denoted that diode with BHSHNI had a dielectric constant of 2.75 at 2000 Hz. A sudden dip in the dielectric constant values observed at higher frequencies could be due to the inability of the interfacial states and minor charges to respond to the AC current. The dielectric loss was calculated and exhibited in Fig. 5e. The lower dielectric loss specified a better dielectric nature of the device. The frequency-dependent AC conductivity was further calculated and plotted as presented in Fig. 5f, and the value was found to be ~ 0.4 $n\Omega^{-1}$ cm^{-1} at higher frequencies.

Generally, most organic materials have a weak UV absorption coefficient, which implies that they do not absorb much UV light, resulting in a poor UV photo-response. Moreover, stability of the organic material can also hinder the UV photodetection. Since UV radiation has high energy and has the potential to photodegrade organic materials, the device performance will eventually deteriorate. Because of this, employing organic materials for UV photodetection applications is not always preferable.

Hybrid Diode Fabrication

As there was no light response from the organic diode, conventionally used *p*-type PEDOT:PSS was replaced with NiO as an electron-blocking layer and BHSHNI as the *n*-type material to construct an inorganic–organic hybrid *p–n* type diode. The device architecture and the energy level diagram are displayed in Fig. 4a and b, respectively. The photo-response of the diode was checked by coating NiO (~ 200 nm) as the *p*-type material on the ITO plate using magnetron sputtering. The sputtered NiO was confirmed using XRD patterns as displayed in Fig. S7. The experimentally obtained XRD patterns were compared with the theoretically obtained XRD patterns. BHSHNI (250 nm) was thermal evaporated on NiO with an evaporation rate of 0.1–0.5 Å/s. Al as cathode was coated above BHSHNI under a vacuum of 6×10^{-6} mbar with an evaporation rate of 1–5 Å/s and diode characteristics were measured. The ideality factors calculated for the diode in dark and visible light were found to be 9.341 and 15.275, respectively (Fig. 6a and b). It is evident from the I–V curve that there is almost a 10-fold increase in the current value when light is incident on the device. This could be due to the high air stability, hole conductivity, and LUMO level for blocking the external electrons injection of the metal-oxide layer.
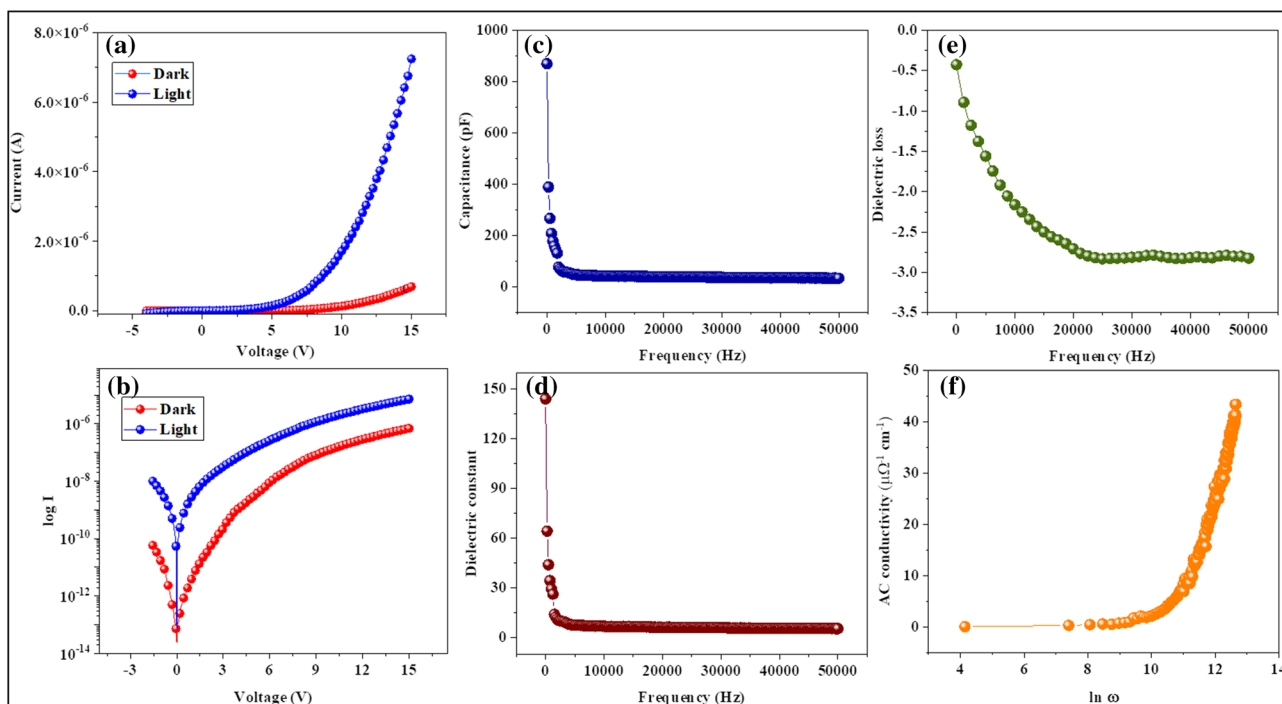
Fig. 6 Plots of (a) I–V, (b) log I versus V in light and dark conditions, (c) capacitance against frequency, (d) dielectric constant against frequency, (e) dielectric loss against frequency and (f) AC conductivity against logarithm of angular frequency for the hybrid diode.

Dielectric measurement of the hybrid diode was performed at 10–50 kHz and the capacitance versus frequency graph exhibited a capacitance value of ~ 39 pF at 30 kHz (Fig. 6c). The frequency dependent dielectric constant was found to be ~ 7.65 at 30 kHz as displayed in Fig. 6d and the negative dielectric loss denotes higher charge storing capacity of the diode (Fig. 6e). The AC conductivity was ~ 45 $\mu\Omega^{-1}$ cm^{-1} at higher frequencies (Fig. 6f).

In order to understand the transport of charges, Nyquist plot was drawn. Grain boundaries, bulk grains, electrode-film interfaces and their response to the AC current was studied using circuit.[50] The Nyquist plot with the fitted circuit is depicted in Fig. 7, which denotes the contact resistance (R_s) to be 1.58×10^4 Ω with charge transfer resistance (R_{ct}) of 1.65×10^6 Ω and a capacitance of 7.06×10^{-11} F, which is in accordance with the dielectric values. The absence of semicircle nature in the plot is indicative of lower charge storing capacity and higher resistance of the system.

In comparison to the organic diode, the hybrid diode not only exhibited a higher current value in the I–V plot in presence of light, but also exhibited better current in dark conditions with comparatively same ideality factor. Further, the photo-responsivity (R) was calculated using Eq. 4,

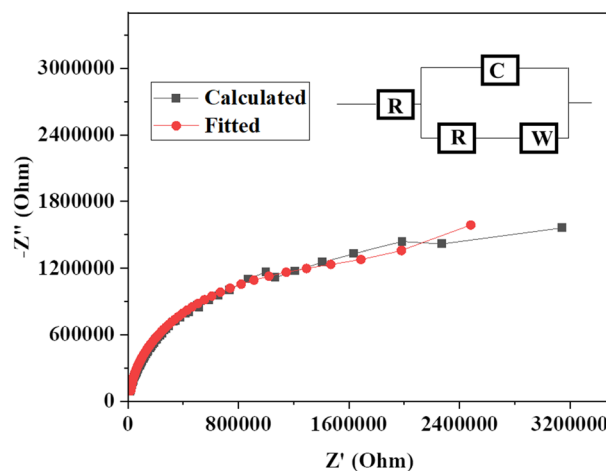$$R = \frac{I_{illuminated} - I_{dark}}{P_{illuminated}} \; (A/W) \qquad (4)$$

Fig. 7 Nyquist plot with circuit fit for hybrid system.

where $I_{illuminated}$ is the current signal under illumination and I_{dark} indicates the dark current and P is the optical power density of the photodetector when the light illuminated the device area A. The responsivity of the hybrid diode was calculated to be 66.26 μA/W. Further, to obtain a high R value, it is essential to have a high photo current under light illumination, which was not observed in our device. However, in comparison to the organic diode, the hybrid diode exhibited a better photo current in the presence of light. The working

mechanism of the device is as follows: after the UV light falls on the device, excitons are created in the *p–n* junction. The internal built in electric field separates the electrons and holes which drift towards respective electrodes. In the space charge region, built-in photogenerated charge carriers are drifted by the internal electric field. Therefore, photocurrent can increase under reverse bias as observed in our study.

Conclusion

A naphthalimide derivative BHSHNI was synthesized through bromination and imidation reactions from 3-hydroxy-1,8-naphthalic anhydride and was characterized using IR, NMR, and mass spectrometry. The ICT within the molecule was validated using both theoretical and experimental studies. The *n*-type semiconductor displayed good thermal stability with an electrochemical band gap of 1.1 eV. A hybrid diode was fabricated by replacing PEDOT:PSS with NiO, which exhibited a photo-response. The dielectric studies revealed that the BHSHNI possessed a lower dielectric constant (2.01 at 500 Hz) than that of the organic device (2.75 at 2000 Hz), but the dielectric constant value increased in the hybrid diode. The ideality factors of the organic diode with BHSHNI were 27.6 and 14, whereas that for the hybrid diode were 9.341 and 15.275 in dark and light conditions, respectively. The hybrid diode can be further explored for photo-sensing applications.

References

1. A.F. Paterson, S. Singh, K.J. Fallon, T. Hodsden, Y. Han, B.C. Schroeder, H. Bronstein, M. Heeney, I. McCulloch, and T.D. Anthopoulos, Recent progress in high-mobility organic transistors: a reality check. *Adv. Mater.* 30, 1–33 (2018). https://doi.org/10.1002/adma.201801079.

2. Y. Gong, X. Zhan, Q. Li, and Z. Li, Progress of pyrene-based organic semiconductor in organic field effect transistors. *Sci. China Chem.* 59, 1623–1631 (2016). https://doi.org/10.1007/s11426-016-0392-7.

3. Q.F. Li, S. Liu, H.Z. Chen, and H.Y. Li, Alignment and patterning of organic single crystals for field-effect transistors. *Chin. Chem. Lett.* 27, 1421–1428 (2016). https://doi.org/10.1016/j.cclet.2016.06.027.

4. Y.Q. Zheng, J.Y. Wang, and J. Pei, One-dimensional (1D) micro/nanostructures of organic semiconductors for field-effect transistors. *Sci. China Chem.* 58, 937–946 (2015). https://doi.org/10.1007/s11426-015-5410-1.

5. L. Lu, T. Zheng, Q. Wu, A.M. Schneider, D. Zhao, and L. Yu, Recent advances in bulk heterojunction polymer solar cells. *Chem. Rev.* 115, 12666–12731 (2015). https://doi.org/10.1021/acs.chemrev.5b00098.

6. G. Li, R. Zhu, and Y. Yang, Polymer solar cells. *Nat. Photonics* 6, 153–161 (2012). https://doi.org/10.1038/nphoton.2012.11.

7. Y. Li, W.K. Tatum, J.W. Onorato, S.D. Barajas, Y.Y. Yang, and C.K. Luscombe, An indacenodithiophene-based semiconducting polymer with high ductility for stretchable organic electronics. *Polym. Chem.* 8, 5185–5193 (2017). https://doi.org/10.1039/c7py00435d.

8. N.T. Kalyani and S.J. Dhoble, Novel materials for fabrication and encapsulation of OLEDs. *Renew. Sustain. Energy Rev.* 44, 319–347 (2015). https://doi.org/10.1016/j.rser.2014.11.070.

9. Q. Li, Y. Guo and Y. Liu, Exploration of near-infrared organic photodetectors. *Chem. Mater.* 31, 6359–6379 (2019). https://doi.org/10.1021/acs.chemmater.9b00966.

10. H. Ren, J. De Chen, Y.Q. Li, and J.X. Tang, Recent progress in organic photodetectors and their applications. *Adv. Sci.* 8, 1–23 (2021). https://doi.org/10.1002/advs.202002418.

11. W. Zhao, Z. He, J.W.Y. Lam, Q. Peng, H. Ma, Z. Shuai, G. Bai, J. Hao, and B.Z. Tang, Rational molecular design for achieving persistent and efficient pure organic room-temperature phosphorescence. *Chem* 1, 592–602 (2016). https://doi.org/10.1016/j.chempr.2016.08.010.

12. T. Lin and J. Wang, Strategies toward high-performance solution-processed lateral photodetectors. *Adv. Mater.* 31, 1–18 (2019). https://doi.org/10.1002/adma.201901473.

13. S. Chen, P. Zeng, X. Wang, X. Wu, P. Lin, and Z. Peng, Naphthalimide-arylamine derivatives with aggregation induced delayed fluorescence for realizing efficient green to red electroluminescence. *J. Mater. Chem. C* 7, 2886–2897 (2019). https://doi.org/10.1039/C8TC06163G.Volume.

14. Y. Liu, F. Niu, J. Lian, P. Zeng, and H. Niu, Synthesis and properties of starburst amorphous molecules: 1,3,5-Tris(1,8-naphthalimide-4-yl)benzenes. *Synth. Met.* 160, 2055–2060 (2010). https://doi.org/10.1016/j.synthmet.2010.07.020.

15. D. Kolosov, V. Adamovich, P. Djurovich, and M.E. Thompson, 1, 8-Naphthalimides in phosphorescent organic LEDs: the interplay between dopant, exciplex, and host emission. *J. Am.*

Chem. Soc. 124, 9945–9954 (2002). https://doi.org/10.1021/ja0263588.

16. H. Ulla, M.R. Kiran, B. Garudachari, T.N. Ahipa, K. Tarafder, A.V. Adhikari, G. Umesh, and M.N. Satyanarayan, Blue emitting 1,8-naphthalimides with electron transport properties for organic light emitting diode applications. *J. Mol. Struct.* 1143, 344–354 (2017). https://doi.org/10.1016/j.molstruc.2017.04.103.

17. W. Jiang, Y. Sun, X. Wang, Q. Wang, and W. Xu, Synthesis and photochemical properties of novel 4-diarylamine-1,8-naphthalimide derivatives. *Dyes Pigments* 77, 125–128 (2008). https://doi.org/10.1016/j.dyepig.2007.03.017.

18. P. Xiao, F. Dumur, B. Graff, D. Gigmes, J.P. Fouassier, and J. Lalevée, Blue light sensitive dyes for various photopolymerization reactions: naphthalimide and naphthalic anhydride derivatives. *Macromolecules* 47, 601–608 (2014). https://doi.org/10.1021/ma402376x.

19. J. Zhang, H. Xiao, X. Zhang, Y. Wu, G. Li, C. Li, X. Chen, W. Ma, and Z. Bo, 1,8-Naphthalimide-based nonfullerene acceptors for wide optical band gap polymer solar cells with an ultrathin active layer thickness of 35 nm. *J. Mater. Chem. C.* 4, 5656–5663 (2016). https://doi.org/10.1039/c6tc01438k.

20. S. Saha and A. Samanta, Influence of the structure of the amino group and polarity of the medium on the photophysical behavior of 4-amino-1,8-naphthalimide derivatives. *J. Phys. Chem. A.* 106, 4763–4771 (2002). https://doi.org/10.1021/jp013287a.

21. D.M. Han, H.J. Song, C.H. Han, and Y.S. Kim, Enhancement of the outdoor stability of dye-sensitized solar cells by a spectrum conversion layer with 1,8-naphthalimide derivatives. *RSC Adv.* 5, 32588–32593 (2015). https://doi.org/10.1039/c5ra03908h.

22. W. Zhu, L. Song, Y. Yang, and H. Tian, Novel bisthienylethene containing ferrocenyl-substituted naphthalimide: a photo- and redox multi-addressable molecular switch. *Chem. A Eur. J.* 18, 13388–13394 (2012). https://doi.org/10.1002/chem.201202189.

23. Y. Wang, X. Zhang, B. Han, J. Peng, S. Hou, Y. Huang, H. Sun, M. Xie, and Z. Lu, The synthesis and photoluminescence characteristics of novel blue light-emitting naphthalimide derivatives. *Dyes Pigments* 86, 190–196 (2010). https://doi.org/10.1016/j.dyepig.2010.01.003.

24. N.V. Marinova, N.I. Georgiev, and V.B. Bojinov, Facile synthesis, sensor activity and logic behaviour of 4-aryloxy substituted 1,8-naphthalimide. *J. Photochem. Photobiol. A Chem.* 254, 54–61 (2013). https://doi.org/10.1016/j.jphotochem.2013.01.008.

25. P. Gąsiorski, K.S. Danel, M. Matusiewicz, T. Uchacz, W. Kuźnik, Ł Piątek, and A.V. Kityk, DFT/TDDFT study on the electronic structure and spectral properties in annulated analogue of phenyl heteroazulene derivative. *Mater. Chem. Phys.* 132, 330–338 (2012). https://doi.org/10.1016/j.matchemphys.2011.11.025.

26. A.V. Kityk, Absorption and fluorescence spectra of heterocyclic isomers from long-range-corrected density functional theory in polarizable continuum approach. *J. Phys. Chem. A.* 116, 3048–3055 (2012). https://doi.org/10.1021/jp300305j.

27. Y. Xue, J. Mou, Y. Liu, X. Gong, Y. Yang, and L. An, An ab initio simulation of the UV/Visible spectra of substituted chalcones. *Cent. Eur. J. Chem.* 8, 928–936 (2010). https://doi.org/10.2478/s11532-010-0058-3.

28. Y. Xue and X. Gong, The conformational, electronic and spectral properties of chalcones: a density functional theory study. *J. Mol. Struct. THEOCHEM.* 901, 226–231 (2009). https://doi.org/10.1016/j.theochem.2009.01.034.

29. S. Hamai and F. Hirayama, Actinometric determination of absolute fluorescence quantum yields. *J. Phys. Chem.* 87, 83–89 (1983). https://doi.org/10.1021/j100224a020.

30. J.A. Osaheni and S.A. Jenekhe, Efficient blue luminescence of a conjugated polymer exciplex. *Macromolecules* 27, 739–742 (1994). https://doi.org/10.1021/ma00081a018.

31. A. Mahajan, R.K. Aulakh, R.K. Bedi, S. Kumar, S. Kumar, and D.K. Aswal, Synthesis and characterization of excited state intramolecular proton transfer based 2-hydroxylaryl imidazole fluorescent materials. *Synth. Met.* 162, 58–63 (2012). https://doi.org/10.1016/j.synthmet.2011.11.009.

32. S. Poojary, D. Sunil, D. Kekuda, and S. Sreenivasa, Fluorescent aromatic symmetrical azines: Synthesis and appraisal of their photophysical and electrochemical properties. *Opt. Mater. (Amst)* 85, 1–7 (2018). https://doi.org/10.1016/j.optmat.2018.08.020.

33. H.E. Katz, A.J. Lovinger, J. Johnson, C. Kloc, T. Siegrist, W. Li, Y.Y. Lin, and A. Dodabalapur, A soluble and air-stable organic semiconductor with high electron mobility. *Nature* 404, 478–481 (2000). https://doi.org/10.1038/35006603.

34. Z. Xu, X. Qian, J. Cui, and R. Zhang, Exploiting the deprotonation mechanism for the design of ratiometric and colorimetric Zn^{2+} fluorescent chemosensor with a large red-shift in emission. *Tetrahedron* 62, 10117–10122 (2006). https://doi.org/10.1016/j.tet.2006.08.050.

35. F.M. Pfeffer, A.M. Buschgens, N.W. Barnett, T. Gunnlaugsson, and P.E. Kruger, 4-Amino-1,8-naphthalimide-based anion receptors: employing the naphthalimide N-H moiety in the cooperative binding of dihydrogenphosphate. *Tetrahedron Lett.* 46, 6579–6584 (2005). https://doi.org/10.1016/j.tetlet.2005.07.067.

36. W. Zhu, Y. Xu, Y. Zhang, J. Shen, and H. Tian, Singlet energy transfer and photoinduced electron transfer in star-shaped naphthalimide derivatives based on triphenylamine. *Bull. Chem. Soc. Jpn.* 78, 1362–1367 (2005). https://doi.org/10.1246/bcsj.78.1362.

37. Z. Xie, B. Yang, G. Cheng, L. Liu, F. He, F. Shen, and Y. Ma, Supramolecular interactions induced fluorescence in crystal: anomalous emission of 2, 5-diphenyl-1, 4-distyrylbenzene with all cis double bonds. *Communications* 17, 1287–1289 (2005). https://doi.org/10.1021/cm048400z.

38. Y. Dong, B. Xu, J. Zhang, X. Tan, L. Wang, J. Chen, H. Lv, S. Wen, B. Li, L. Ye, B. Zou, and W. Tian, Piezochromic luminescence based on the molecular aggregation of 9,10-Bis((*E*)-2-(pyrid-2-yl)vinyl)anthracene. *Angew. Chem. Int. Ed.* 51, 10782–10785 (2012). https://doi.org/10.1002/anie.201204660.

39. H. Ulla, B. Garudachar, M.N. Satyanarayan, G. Umesh, A.M. Isloor, Blue light emitting naphthalimides for organic light emitting diodes, in *AIP Conference Proceedings*, vol. 1512, pp. 1300–1301 (2013). https://doi.org/10.1063/1.4791530

40. J. Liu, Y. Li, Y. Wang, H. Sun, Z. Lu, H. Wu, J. Peng, and Y. Huang, Synthesis and luminescent properties of blue sextuple-hydrogen-bond self-assembly molecular duplexes bearing 4-phenoxy-1,8-naphthalimide moieties. *Opt. Mater. (Amst)* 34, 1535–1542 (2012). https://doi.org/10.1016/j.optmat.2012.03.022.

41. H. Ulla, B. Garudachar, M.N. Satyanarayan, G. Umesh, A.M. Isloor, Blue light emitting materials for organic light emitting diodes: Experimental and simulation study, in *International Conference on Optical Engineering (ICOE)*, vol. 978, pp. 6–9. (2012). https://doi.org/10.1109/ICOE.2012.6409561

42. G. Ding, Z. Xu, G. Zhong, S. Jing, F. Li, and W. Zhu, Synthesis, photophysical and electroluminescent properties of novel naphthalimide derivatives containing an electron-transporting unit. *Res. Chem. Intermed.* 34, 299–308 (2008). https://doi.org/10.1163/156856708783623401.

43. W. Zhang, Y. Xu, M. Hanif, S. Zhang, J. Zhou, D. Hu, Z. Xie, and Y. Ma, Enhancing fluorescence of naphthalimide derivatives by suppressing the intersystem crossing. *J. Phys. Chem. C.* 121, 23218–23223 (2017). https://doi.org/10.1021/acs.jpcc.7b07513.

44. P. Ledwon, A. Brzeczek, S. Pluczyk, T. Jarosz, W. Kuznik, K. Walczak, and M. Lapkowski, Synthesis and electrochemical properties of novel, donor-acceptor pyrrole derivatives with 1,8-naphthalimide units and their polymers. *Electrochim. Acta*

128, 420–429 (2014). https://doi.org/10.1016/j.electacta.2013.10.163.

45. P. Chattopadhyay and B. RayChaudhuri, Frequency dependence of forward capacitance-voltage characteristics of Schottky barrier diodes. *Solid State Electron.* 36, 605–610 (1993). https://doi.org/10.1016/0038-1101(93)90272-R.

46. Y. Lee, J. Lee, and J. Park, Dielectric phenomena of an organic light emitting diode. *Mol. Cryst. Liq. Cryst. Sci. Technol. Sect. A. Mol. Cryst. Liq. Cryst.* 370, 73–76 (2001). https://doi.org/10.1080/10587250108030042.

47. G. Nyström, A. Razaq, M. Strømme, L. Nyholm, and A. Mihranyan, Ultrafast all-polymer paper-based batteries. *Nano Lett.* 9, 3635–3639 (2009). https://doi.org/10.1021/nl901852h.

48. S. Ummartyotin and H. Manuspiya, A critical review on cellulose: From fundamental to an approach on sensor technology. *Renew. Sustain. Energy Rev.* 41, 402–412 (2015). https://doi.org/10.1016/j.rser.2014.08.050.

49. E.M. Godzhaev, A.M. Magerramov, S.S. Osmanova, M.A. Nuriev, and E.A. Allakhyarov, Charge state of composites based on polyethylene with semiconductor filler $TlInSe_2$. *Surf. Eng. Appl. Electrochem.* 43, 148–151 (2007). https://doi.org/10.3103/s1068375507020160.

50. S. Saha and S.B. Krupanidhi, Dielectric response in pulsed laser ablated $(Ba, Sr)TiO_3$ thin films. *J. Appl. Phys.* 87, 849–854 (2000). https://doi.org/10.1063/1.371952.